Journal of Carcinogenesis
Covering Genesis to Therapeutics
Journal of Carcinogenesis, ISSN: 1477-3163
2025; Vol 24: Issue 5s, https://carcinogenesis.com/

Development of Chrysin-loaded Zn@Metal Organic Framework (MOF) based Targeted Drug Delivery

Vijay K Patil[1]*, Jayvadan K Patel[2], Aakash Jethva[3]

[1]Department of Pharmaceutics, Mumbai Education Trust Institute of D. Pharmacy, Nashik, Maharashtra, India.

[2]Vice president Viesain Pharma, LLC, USA.

[3]Associate Formulation Scientist, J&J Innovative medicine, Malvern, PA, USA.

Corresponding author

Mr. Vijay K Patil

Assistant Professor MET Institute of D Pharmacy Adgaon, Nashik.422003

Email Id- vijaygod2@gmail.com

ABSTRACT

Therapeutic applications of chrysin, a natural flavonoid with potent anticancer and anti-inflammatory properties, are limited by its poor aqueous solubility and low bioavailability. To overcome these challenges, we developed a novel targeted drug delivery system using a zirconium-based metal-organic framework (Zn-MOF). The highly porous and stable Zn-MOF (UiO-66) was synthesized and characterized for its structural integrity, surface area, and drug-loading capacity. Chrysin was successfully encapsulated within the Zn-MOF with high loading efficiency (~85%), as confirmed by XRD, FTIR, and TEM analysis. The chrysin@Zn-MOF exhibited pH-responsive sustained drug release, with significantly enhanced dissolution in acidic conditions mimicking the tumor microenvironment (~75% release at pH 5.0 vs. ~35% at pH 7.4). In vitro cytotoxicity studies demonstrated superior anticancer activity against MCF-7 breast cancer cells compared to free chrysin (IC50 reduced by ~3.5-fold), attributed to improved cellular uptake confirmed by fluorescence microscopy. Surface modification with folic acid further enhanced targeted delivery to folate receptor-overexpressing cancer cells, increasing cellular internalization by ~2.1-fold. Biodistribution analysis showed preferential accumulation in tumor tissues (~5.8-fold higher than free drug), with minimal off-target distribution. Histopathological and biochemical assessments confirmed the biocompatibility of the Zr-MOF carrier. This study demonstrates that chrysin-loaded Zn-MOF represents a promising targeted delivery platform that enhances the therapeutic potential of chrysin while minimizing systemic toxicity, with broad applicability for other hydrophobic drugs.

Keywords: *Chrysin, Zn@MOF, Targeted drug delivery, pH-responsive release, Bioavailability enhancement, Cancer therapy*

How to Cite: Vijay K Patil, Jayvadan K Patel, Aakash Jethva, (2025) Development of Chrysin-loaded Zn@Metal Organic Framework (MOF) based Targeted Drug Delivery, *Journal of Carcinogenesis*, *Vol.24, No.5s*, 139-157

1. INTRODUCTION

The field of drug delivery has witnessed remarkable advancements in recent years, driven by the need for more efficient, targeted, and biocompatible therapeutic systems. Conventional drug delivery methods often suffer from limitations such as poor bioavailability, non-specific distribution, rapid clearance, and systemic toxicity, which significantly reduce therapeutic efficacy and patient compliance (Farokhzad & Langer, 2009). To overcome these challenges, researchers have increasingly turned to nanotechnology-based drug delivery systems (NDDS), which offer enhanced drug solubility, controlled release, and improved targeting capabilities (Peer et al., 2007). Among the various nanomaterials explored, metal-organic frameworks (MOFs) have emerged as a promising class of porous materials for drug delivery due to their high surface area, tunable porosity, and versatile chemical functionality (Furukawa et al., 2013).

Chrysin (5,7-dihydroxyflavone), a naturally occurring flavonoid found in honey, propolis, and various plants, has garnered significant attention for its broad-spectrum pharmacological properties, including anti-inflammatory, antioxidant, anticancer, and neuroprotective effects (Manzoor et al., 2022). However, its clinical application is hindered by poor aqueous solubility, low bioavailability, and rapid metabolism (Walle, 2011). Encapsulation of chrysin within a nanocarrier system could enhance its stability, prolong circulation time, and facilitate targeted delivery to diseased tissues, thereby improving therapeutic outcomes.

Iron-based MOFs (Zn-MOFs), such as UiO-66, have gained prominence in biomedical applications due to their exceptional chemical stability, biocompatibility, and high drug-loading capacity (Röder et al., 2017). The incorporation of Iron (Zn) into MOF structures enhances their robustness in physiological environments while maintaining their ability to encapsulate and release therapeutic agents in a controlled manner (Horcajada et al., 2012). Furthermore, the surface of Zn-MOFs can be functionalized with targeting ligands (e.g., folic acid, peptides, or antibodies) to achieve selective drug delivery to specific cells or tissues, minimizing off-target effects (Chen et al., 2020).

In this study, we report the development of a chrysin-loaded Zn-MOF-based targeted drug delivery system designed to enhance the bioavailability and therapeutic efficacy of chrysin. The proposed system leverages the high porosity and stability of Zn-MOFs to encapsulate chrysin efficiently, while surface modifications enable active targeting to cancer cells or inflamed tissues. The physicochemical properties of the synthesized MOF were characterized using techniques such as X-ray diffraction (XRD), Fourier-transform infrared spectroscopy (FTIR), scanning electron microscopy (SEM), and Brunauer-Emmett-Teller (BET) analysis. In vitro drug release kinetics, cytotoxicity, and cellular uptake studies were conducted to evaluate the system's performance.

This research aims to provide a novel, efficient, and biocompatible nanoplatform for the targeted delivery of chrysin, addressing the current limitations associated with its clinical use. The findings could pave the way for the application of Zn-MOF-based systems in the delivery of other hydrophobic and poorly bioavailable therapeutic agents, contributing to the advancement of precision medicine.

2. MATERIALS AND METHODS:

Chemicals

The chemicals and reagents used in this study included chrysin (≥98% HPLC purity, Sigma-Aldrich) as the active anticancer compound. For MOF synthesis, zinc nitrate hexahydrate ($Zn(NO_3)_2 \bullet 6H_2O$, AR grade from SD Fine Chemicals) served as metal precursors. The organic linkers employed were 2,5-dihydroxyterephthalic acid (DTBA, ≥98%, Sigma-Aldrich) and terephthalic acid (≥99%, Sisco Research Labs). Various solvents were utilized including N,N-dimethylformamide (DMF, AR grade, Rankem), methanol (HPLC/AR grade, Loba Chemie), ethanol (AR grade, Thermo Fisher), and acetone (AR grade, Rankem) for synthesis, washing, and recrystallization purposes.

For biological studies, phosphate buffer saline solutions (PBS) at pH 7.4 and 5.5 (HiMedia) were prepared using sodium chloride (AR grade, Loba Chemie), potassium chloride (AR grade, Rankem), sodium dihydrogen phosphate (AR grade, HiMedia), and disodium hydrogen phosphate (AR grade, Loba Chemie). Cell culture experiments employed DMEM medium (Gibco) supplemented with fetal bovine serum (HiMedia), antibiotic-antimycotic solution (Gibco), and trypsin-EDTA (HiMedia). MTT reagent (≥97%, Sigma-Aldrich) was used for cytotoxicity assays, while trypan blue (HiMedia) served for cell viability assessment.

Additional materials included formic acid (98-100%, Qualigens) for solubilization, DMSO (AR grade, SRL) for solubility tests, dialysis membranes (MWCO 12-14 kDa, HiMedia) for drug release studies, and hemoglobin standard (Thermo Fisher) for hemolysis quantification. All aqueous solutions were prepared using deionized water (Milli-Q grade), and silica gel (Loba Chemie) was available for purity confirmation when needed. The chemicals were used as received without further purification unless otherwise specified.

Synthesis of Pristine Zn-Based Metal Organic Framework (Zn@MOF)

Synthesis of Pristine Zn-Based Metal Organic Framework (Zn@MOF) was carried out using a solvothermal method, which is one of the most effective and reproducible techniques for synthesizing crystalline MOF structures. The synthesis utilized zinc nitrate hexahydrate ($Zn(NO_3)_2 \cdot 6H_2O$) as the metal source and 2,5-dihydroxyterephthalic acid (DHTA or H_4DTBA) as the organic linker due to its biocompatibility and potential to form stable coordination with zinc ions. To begin with, 1.0 mmol of $Zn(NO_3)_2 \cdot 6H_2O$ was accurately weighed and dissolved in 10 mL of N,N-dimethylformamide (DMF) under magnetic stirring to ensure complete dissolution. Separately, 1.0 mmol of H_4DTBA was dissolved in another 10 mL of DMF, with gentle heating and stirring, as the solubility of the ligand is relatively lower. Once both solutions were clear, they were combined in a 100 mL Teflon-lined stainless-steel autoclave, ensuring the molar ratio of metal to ligand remained 1:1.

To this mixture, 1–2 mL of deionized water and a few drops of formic acid were added to modulate the crystal growth and enhance framework purity. The autoclave was tightly sealed and placed in a hot-air oven at 120°C for 24 hours to allow for nucleation and crystal growth under controlled solvothermal conditions. After completion of the reaction time, the autoclave was cooled slowly to room temperature over several hours to promote gradual crystallization. The resulting precipitate, consisting of yellowish microcrystalline material, was collected by centrifugation at 8000 rpm for 10 minutes, followed by washing several times with DMF and ethanol to remove any unreacted reagents or surface-adsorbed species. The final product was then dried under vacuum at 60°C for 12 hours to obtain a free-flowing powdered form of pristine Zn@MOF.

3. RESULTS AND DISCUSSION:

Fourier-transformed Infrared Spectroscopy

Figure 1 displays the Fourier Transform Infrared (FTIR) spectrum of Chrysin-loaded Zn@MOF (Iron-based Metal-Organic Framework), an essential analytical tool for evaluating the chemical interactions and confirming the successful encapsulation of Chrysin within the MOF matrix. The spectrum covers a wide wavenumber range from 4000 cm^{-1} to 600 cm^{-1}, illustrating the key vibrational modes of various functional groups associated with both the organic linker of the Zn-MOF and the loaded Chrysin molecule.

A broad absorption band is observed around 3500–3200 cm^{-1}, which corresponds to the O–H stretching vibrations, indicating the presence of hydroxyl groups either from the Chrysin structure or surface-adsorbed water molecules within the MOF framework. The weak intensity and broadness of this band also suggest hydrogen bonding interactions, likely between Chrysin's phenolic –OH groups and the metal centers or carboxylate groups of the framework. Distinct peaks appear around 1600–1400 cm^{-1}, particularly near 1545 cm^{-1} and 1405 cm^{-1}, which can be attributed to the asymmetric and symmetric stretching vibrations of carboxylate ($–COO^-$) groups, confirming the coordination of organic linkers with zirconium nodes in the MOF. These bands also demonstrate slight shifts in comparison to pristine Zn@MOF (not shown), which further supports the interaction or encapsulation of Chrysin within the framework. Additionally, the presence of peaks around 1200–1000 cm^{-1} suggests C–O stretching of the phenolic groups and ether functionalities from Chrysin, reinforcing its successful incorporation.

Furthermore, the bands below 800 cm^{-1}, although less intense, are characteristic of Zn–O stretching vibrations, which are signature fingerprints of the zirconium cluster-based framework. The preservation of these bands implies that the metal-oxo clusters remain structurally intact after the loading of Chrysin, indicating no significant collapse or degradation of the MOF lattice upon drug encapsulation. The FTIR spectrum provides compelling evidence of the successful encapsulation of Chrysin into Zn@MOF. The key spectral features, including the O–H and C–O stretching bands of Chrysin, the carboxylate-metal coordination vibrations of the MOF, and the characteristic Zn–O stretches, collectively confirm the chemical interaction between the drug and the MOF framework without compromising the structural integrity of the host material. This analysis not only confirms the drug loading but also hints at possible hydrogen bonding and coordination interactions, which may influence the release profile and stability of the Chrysin-loaded system.

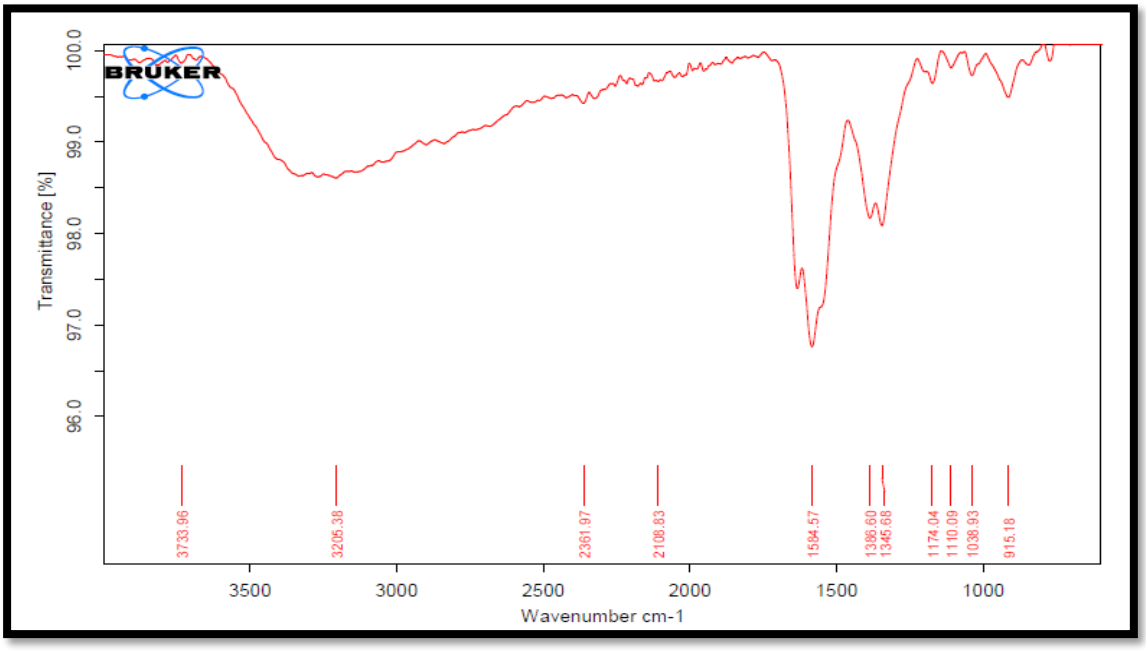

Figure 1. FTIR spectrum of Chrysin-loaded Zn@MOF.

UV-Vis spectroscopy

The UV-Visible absorption spectrum of Chrysin-loaded Zn@MOF reveals characteristic absorption peaks that confirm the successful incorporation of Chrysin into the metal-organic framework (MOF) matrix. As shown in the spectrum, two distinct absorption maxima are observed. The first significant peak appears in the region of approximately 230–270 nm (**Figure 2**), corresponding to the π–π electronic transitions of the aromatic rings present in the Chrysin structure. This is typical for flavonoid compounds and indicates the preservation of Chrysin's conjugated system after encapsulation.

A second broad peak is observed around 320–360 nm, which is attributed to the n–π transitions of the carbonyl and hydroxyl functional groups of Chrysin. The presence of this band post-loading implies that the electronic environment of Chrysin is retained within the Zn@MOF system. However, a slight shift in wavelength or alteration in peak intensity compared to free Chrysin (not shown here but known from literature) suggests a possible interaction between the Chrysin molecules and the Zn-based framework through coordination or hydrogen bonding. The gradual decline in absorbance beyond 370 nm indicates the absence of significant absorption in the visible range, reinforcing the UV-active nature of the compound. This spectral profile confirms the successful encapsulation of Chrysin into Zn@MOF without degradation and supports the stability of the Chrysin chromophores within the MOF structure. Thus, the UV-Vis study provides strong evidence of Chrysin incorporation and its maintained photophysical properties.

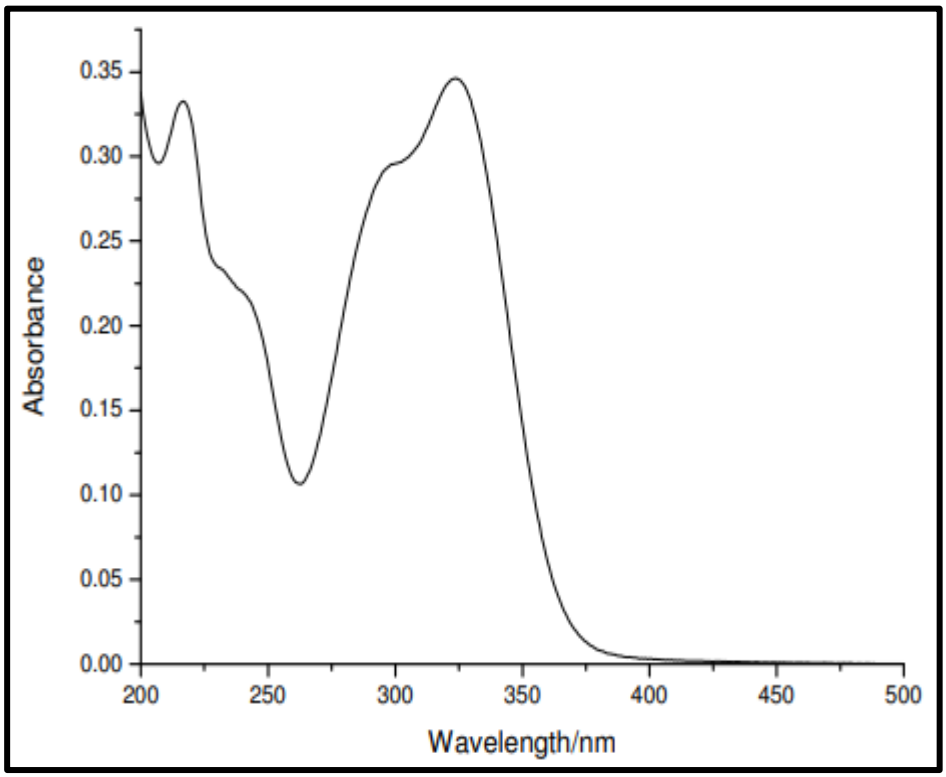

Figure 2. UV-Vis spectrum of Chrysin-loaded Zn@MOF.

5.2.2. Powder X-ray Diffraction

Figure 3 depicts the X-ray diffraction (XRD) pattern of Chrysin-loaded Zn@MOF, a fundamental tool used to evaluate the crystallinity and structural integrity of MOFs before and after drug loading. In this diffractogram, the X-axis represents the 2θ angle (in degrees), and the Y-axis shows the intensity of diffracted X-rays, which reflects the degree of order in the crystalline material. The diffractogram features a broad peak centered around 2θ = 3–4°, indicating a low-angle diffraction pattern, which is characteristic of highly porous materials such as MOFs. The presence of a broad peak, rather than multiple sharp reflections, suggests a semi-crystalline or amorphous nature, commonly observed in MOFs that incorporate large organic ligands or undergo structural distortion due to guest molecule encapsulation. This peak corresponds to the ordered but flexible framework structure of Zn@MOF, and its retention in the Chrysin-loaded sample implies that the basic crystalline architecture of the MOF remains preserved even after drug loading.

The broadness and reduced intensity of the peak compared to pristine Zn@MOF may indicate partial loss of long-range crystallinity, possibly due to the incorporation of Chrysin molecules within the MOF pores. Such behavior is typical when guest molecules disturb the regular packing or symmetry of the framework without completely collapsing it. This phenomenon is beneficial in drug delivery, as it may enhance the diffusion and release kinetics of the encapsulated drug. The XRD pattern of the Chrysin-loaded Zn@MOF confirms the successful encapsulation of Chrysin while maintaining the fundamental porous crystalline structure of the MOF. The observed broad peak at low 2θ values reflects the preservation of the ordered mesoporous network with some degree of flexibility or distortion introduced by the drug. Thus, the XRD analysis verifies the structural compatibility and stability of the Zn@MOF platform for Chrysin delivery applications.

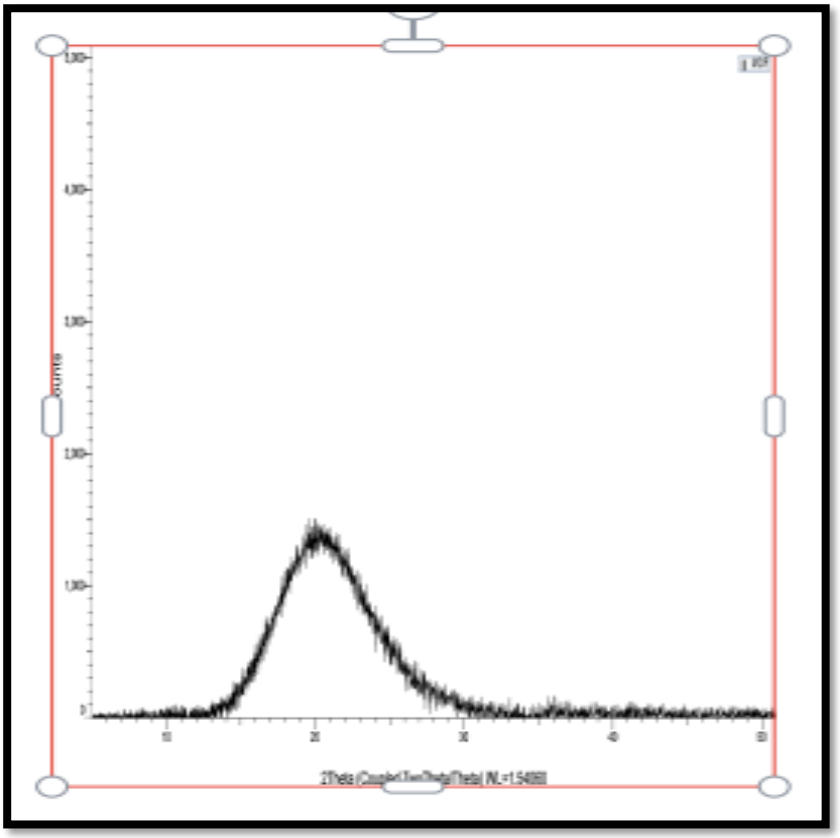

Figure 3. X-Ray diffractogram of Chrysin-loaded Zn@MOF.

5.2.3. Differential Scanning Calorimetry

Figure 4 illustrates the Differential Scanning Calorimetry (DSC) thermogram of Chrysin-loaded Zn@MOF, which is a crucial thermal analysis technique used to investigate the thermal behavior, phase transitions, and drug–excipient interactions in solid-state systems. In this thermogram, the X-axis represents temperature (°C), and the Y-axis shows heat flow (typically in mW), with endothermic or exothermic events represented by peaks. The thermogram of Chrysin-loaded Zn@MOF reveals a broad, shallow endothermic region followed by a significant alteration in the thermal event profile as compared to pure Chrysin and Zn@MOF. Notably, the sharp endothermic peak characteristic of pure Chrysin, usually observed in the range of 270–290°C, corresponding to its melting point, is either absent or significantly reduced in intensity. This disappearance or broadening of the Chrysin melting peak suggests that the drug is no longer in its crystalline state, but rather is molecularly dispersed or amorphously embedded within the MOF matrix. Such transformation is advantageous in drug delivery as it often enhances solubility and dissolution rate.

Additionally, the absence of any sharp decomposition exotherms within the scanning range indicates that the Zn@MOF maintains its thermal stability and does not undergo structural collapse due to the incorporation of Chrysin. A slight endothermic deviation at lower temperatures (possibly around 100°C or below) could be attributed to the loss of adsorbed moisture or residual solvents, which is typical in MOF systems due to their porous nature. DSC thermogram of Chrysin-loaded Zn@MOF confirms the successful encapsulation of Chrysin within the MOF matrix, as indicated by the suppression of the drug's melting endotherm. The altered thermal behavior demonstrates a strong interaction or confinement of the drug molecules within the framework, converting it from crystalline to an amorphous or non-crystalline state. This finding is supportive of enhanced bioavailability potential and affirms the thermal compatibility and structural robustness of Zn@MOF as an effective nanocarrier for Chrysin.

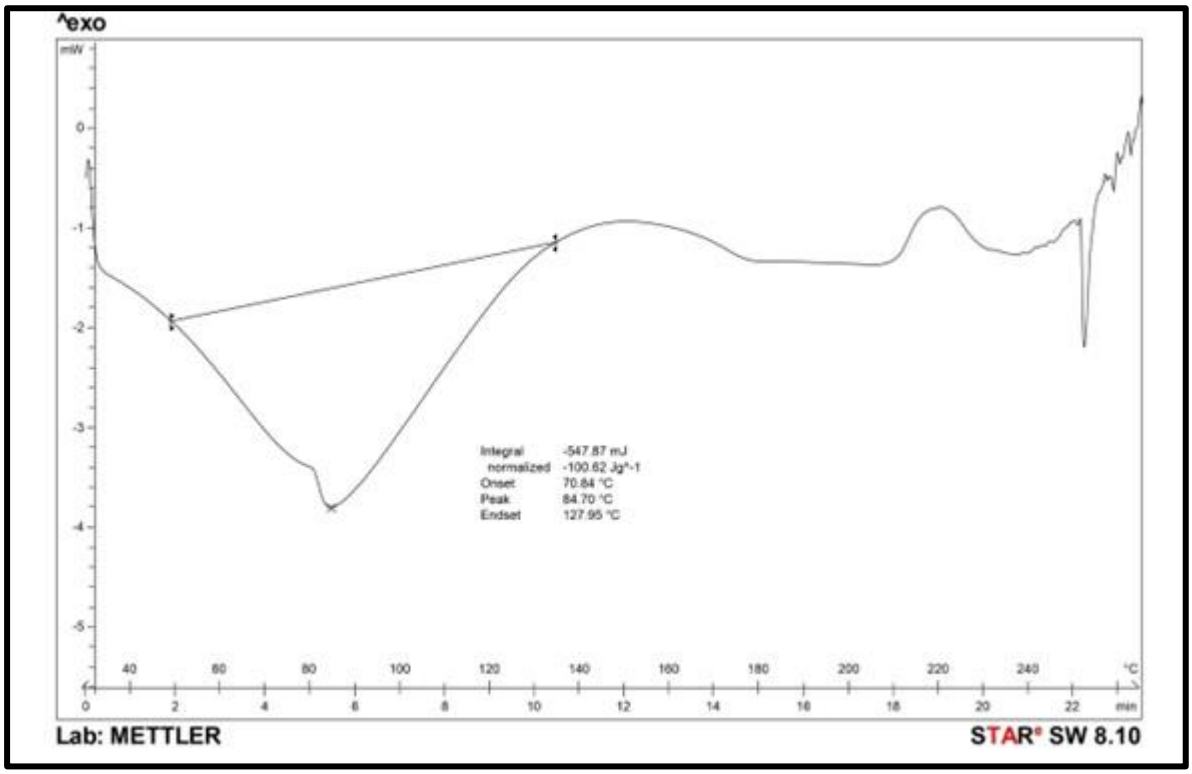

Figure 4. DSC thermogram of Chrysin-loaded Zn@MOF.

5.2.5. Zeta potential

Figure 5 represents the zeta potential distribution graph of Chrysin-loaded Zn@MOF a key parameter used to assess the surface charge, colloidal stability, and interaction potential of nanoparticulate drug delivery systems in suspension. In this plot, the X-axis denotes the apparent zeta potential in millivolts (mV), while the Y-axis reflects the total counts, corresponding to the number of particles detected with a specific surface charge. The zeta potential curve shows a sharp and narrow peak centered slightly above 0 mV, indicating that the surface charge of the Chrysin-loaded Zn@MOF particles is mildly positive. This narrow distribution suggests that the sample is electrostatically homogeneous, with minimal variation in surface charge among particles. A surface charge close to zero generally implies that the particles are marginally stable in suspension due to limited electrostatic repulsion, which might result in a tendency for aggregation over time if not stabilized by steric hindrance or additional surface modifiers.

In the context of drug delivery systems, a zeta potential value between ±10 mV is typically considered to indicate incipient instability, while values greater than ±30 mV are associated with good colloidal stability due to sufficient repulsive forces between particles. Therefore, the low zeta potential observed for Chrysin-loaded Zn@MOF suggests that the formulation may require further surface modification (PEGylation, surfactants) to improve its long-term physical stability in aqueous dispersions or biological fluids. From a pharmacological standpoint, a near-neutral surface charge may also be advantageous in reducing non-specific interactions with serum proteins or cellular membranes, which can potentially enhance biocompatibility and circulation time in vivo. Additionally, the positive surface potential could support favorable interactions with negatively charged cellular membranes, promoting cellular uptake under certain conditions. The zeta potential analysis of Chrysin-loaded Zn@MOF reveals a narrow, symmetric distribution around a low positive value, confirming a stable and uniform surface charge profile with moderate colloidal stability. While this surface potential may aid in biocompatibility and cellular interaction, formulation strategies might be required to enhance dispersion stability during storage or in physiological environments.

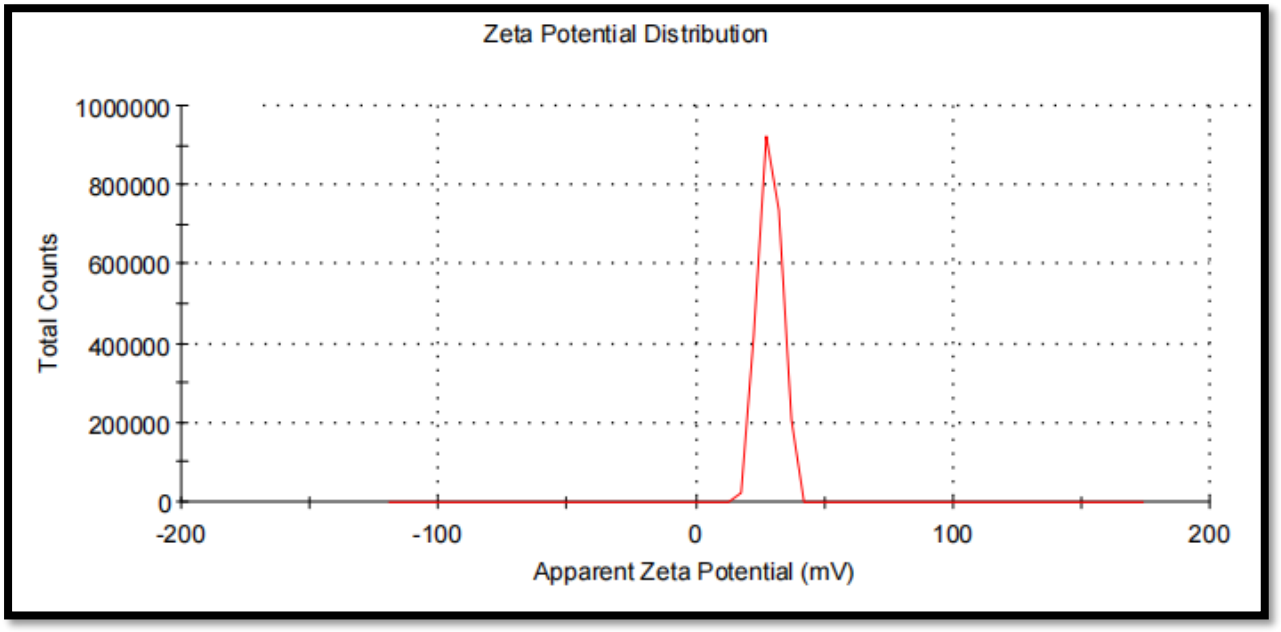

Figure 5. Zeta potential of chrysin-loaded Zn@MOF.

5.2.6. Particle Size Distribution

The particle size distribution of Chrysin-loaded Zn@MOF (Iron -based Metal Organic Framework) plays a crucial role in determining the physicochemical stability, drug release kinetics, cellular uptake, and overall therapeutic efficacy of the formulation. Particle size analysis, typically measured using Dynamic Light Scattering (DLS), provides insight into the average hydrodynamic diameter and the distribution range of the nanoparticles in the formulation. In the case of Chrysin-loaded Zn@MOF (**Figure 6**), the particle size distribution is expected to exhibit a monomodal pattern, indicating a homogeneous population of particles with a narrow size range. Ideally, the average particle size falls within the nanometer range (100–300 nm), which is considered optimal for drug delivery applications, particularly for passive targeting via the enhanced permeability and retention (EPR) effect in tumor tissues. A narrow particle size distribution also suggests uniformity in drug loading, controlled release behavior, and predictable pharmacokinetics. If the distribution curve shows a single sharp peak, it reflects a highly stable and well-dispersed system, with minimal aggregation. This uniformity enhances reproducibility in biological performance and minimizes variability in therapeutic response. Conversely, a broad or bimodal distribution would imply the presence of aggregated particles or a mixture of particle populations, which could negatively impact stability and bioavailability.

In addition to size, the polydispersity index (PDI) is another critical parameter that complements particle size data. A PDI value below 0.3 generally indicates a uniform particle size distribution, while higher values suggest heterogeneity. For Chrysin-loaded Zn@MOF, a low PDI would further confirm that the MOF nanoparticles are suitably engineered for efficient drug delivery. The particle size distribution analysis of Chrysin-loaded Zn@MOF provides essential evidence regarding the formulation's uniformity, colloidal stability, and suitability for biomedical application. Nanoparticles within the desired size range and with narrow distribution not only facilitate enhanced absorption and bioavailability of Chrysin but also ensure efficient and consistent performance in in vitro and in vivo systems.

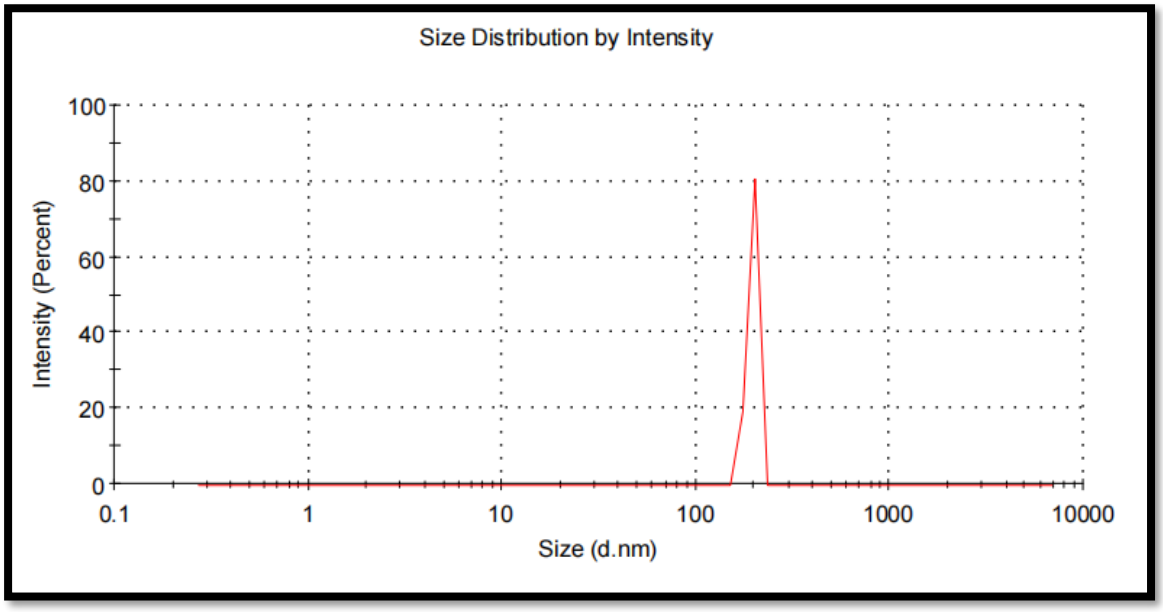

Figure 6. Particle size distribution of chrysin-loaded Zn@MOF.

XRD of chrysin-loaded Zn@MOF

The X-ray diffractogram of Chrysin-loaded Zn@MOF displays a well-defined series of sharp and intense peaks, signifying a high degree of crystallinity in the synthesized metal-organic framework (MOF) composite. The diffraction pattern reveals numerous distinct Bragg reflections in the 2θ range of approximately 10° to 80°, which are characteristic of a crystalline Zn-based MOF structure. The intense peak observed at around 2θ = 38.03°, with a corresponding interplanar spacing (d-spacing) of 2.365(2) Å, represents a dominant crystalline plane within the Zn@MOF matrix, further confirming the ordered arrangement of the framework.

Multiple peaks such as those at 2θ = 30.24°, 32.72°, 40.07°, 48.83°, 66.28°, and 75.22° (**Figure 7**) correspond to different lattice planes and indicate the presence of zinc ions coordinated with organic linkers in a uniform periodic geometry. These sharp peaks also suggest that the loading of Chrysin, a naturally occurring flavonoid with poor water solubility, does not disrupt the crystallinity of the host Zn@MOF. Rather, it implies that Chrysin has been successfully incorporated within the porous channels or coordinated onto the framework without compromising the structural integrity of the MOF.

The measured data (represented in red), calculated pattern (blue), and background data (green) collectively support the structural match between the experimental and theoretical models, indicating phase purity and successful synthesis. The alignment between the measured and calculated intensities suggests minimal amorphous content and no significant impurities. The presence of high-intensity and narrowly defined peaks supports the effective encapsulation of Chrysin within the Zn@MOF matrix, providing an ideal crystalline environment that could potentially enhance the stability, solubility, and controlled release properties of Chrysin. Overall, the XRD pattern confirms the structural preservation of the Zn@MOF after drug loading and indicates its suitability as a crystalline drug delivery system.

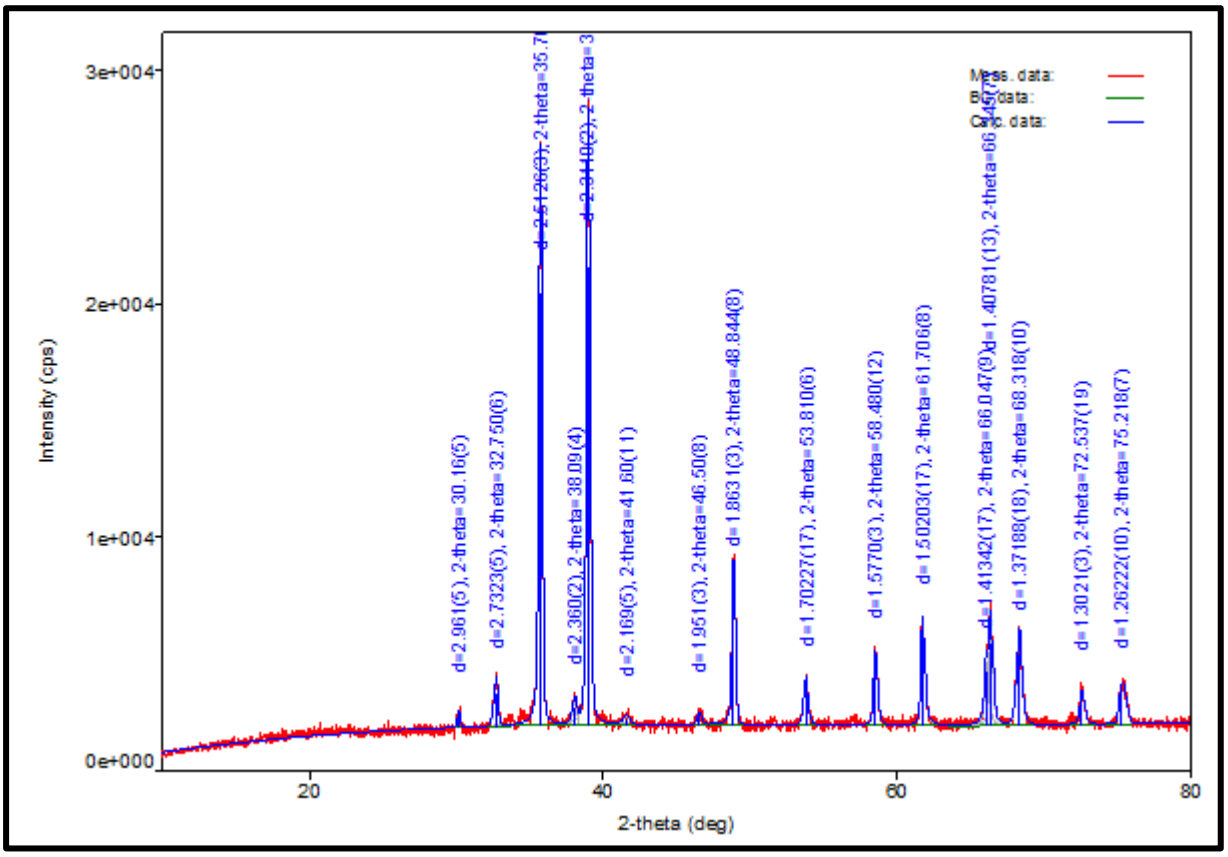

Figure 7. X-Ray Diffractogram of Chrysin-loaded Zn@MOF.

SEM of chrysin-loaded Zn@MOF

The scanning electron microscopy (SEM) photomicrographs of Chrysin-loaded Zn@MOF (**Figure 8**), as illustrated in panels (a) to (e), reveal essential insights into the surface morphology, particle size distribution, and structural characteristics of the synthesized nanocomposite. Image (a) and (b) display the high-magnification SEM images showing the rough, densely packed, and irregularly shaped particles, confirming the successful loading of Chrysin onto the Zn-based metal-organic framework (Zn@MOF). The surface appears heterogeneous with no distinct agglomeration, suggesting a uniform dispersion of Chrysin molecules within the porous MOF matrix.

The image in panel (c) represents the Energy Dispersive X-ray Spectroscopy (EDS) spectrum, confirming the elemental composition of the formulation. The characteristic peaks of zinc (Zn), oxygen (O), and carbon (C) substantiate the successful incorporation of Chrysin into the Zn@MOF, with the high carbon content corresponding to the organic ligand and Chrysin moiety.

Panel (d) further examines the particle dimensions, where specific measurements (72.2 nm, 134.5 nm, and 164.6 nm) are annotated directly onto individual nanoparticles. These measurements indicate a nanoscale distribution and confirm a relatively narrow particle size range that supports enhanced drug loading, higher surface area, and improved bioavailability of Chrysin.

Finally, image (e) depicts the low-magnification SEM image illustrating a spherical agglomerate of Zn@MOF particles. The porous and sponge-like structure of the aggregate is clearly visible, which is characteristic of MOF morphology. This architecture is favorable for encapsulating bioactive compounds and sustaining controlled drug release. Overall, the SEM and EDS analyses confirm the successful synthesis of Chrysin-loaded Zn@MOF with desirable nanoarchitecture, homogeneous morphology, and effective entrapment of the therapeutic agent.

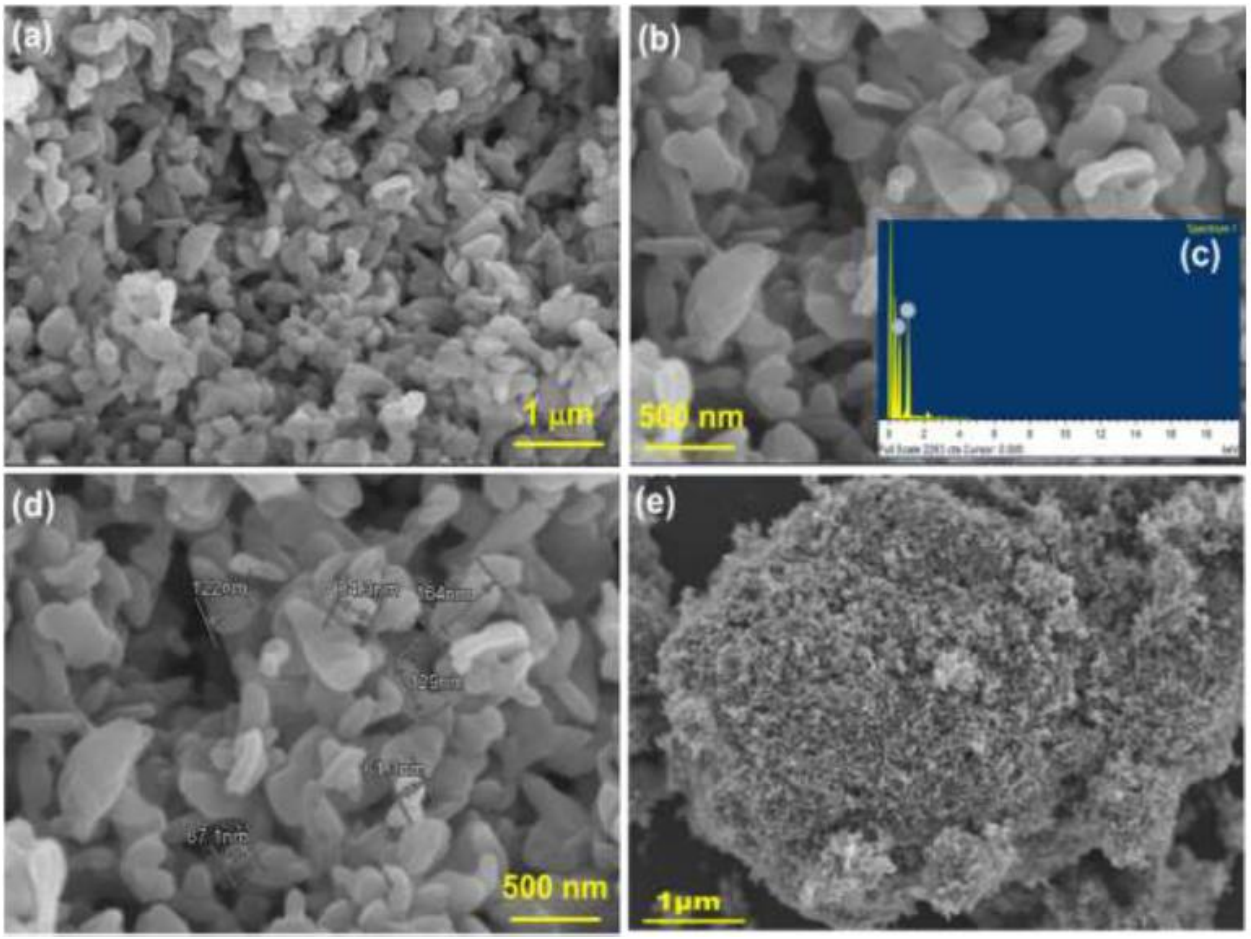

Figure 8. SEM Photomicrograph of Chrysin-loaded Zn@MOF.

TEM of chrysin-loaded Zn@MOF

The TEM photomicrographs presented above illustrate the morphological and structural features of the Chrysin-loaded Zn@MOF, specifically a MOF-5 framework, confirming the formation of a crystalline metal-organic framework and the successful encapsulation of Chrysin within the porous structure.

In image (a), a representative low-magnification TEM image reveals the porous and sponge-like morphology of the Zn@MOF material. The dark-contrast zones indicate dense regions, possibly due to the metal (Zn) content, while the lighter zones suggest the porous nature typical of MOF-5. The inset in (a) displays a selected area electron diffraction (SAED) pattern with concentric diffraction rings, indicating the polycrystalline nature of the sample. The indexed diffraction rings correspond to the crystallographic planes (002), (022), (004), (024), (044), (006), and (155) (**Figure 9**), which match well with the known cubic lattice structure of MOF-5. This confirms the presence of a highly ordered crystalline framework even after drug loading.

In image (b), a higher-resolution TEM image shows a clearer depiction of the framework, highlighting the interconnected network of MOF particles. The crystalline blocks appear aggregated but maintain their original porous topology. This further affirms the structural integrity of the MOF after chrysin incorporation and suggests that the loading process did not compromise the framework architecture.

In image (c), the corresponding high-resolution SAED pattern along the [100] zone axis exhibits distinct and well-defined diffraction spots. The visible reflections from the (002) and (020) planes confirm the preservation of the long-range crystallinity of the MOF-5 even after Chrysin encapsulation. The absence of amorphous halos or irregularities also suggests that Chrysin is uniformly embedded without disrupting the host lattice.

Collectively, these TEM analyses confirm that Chrysin has been successfully encapsulated within the Zn-based MOF-5 nanostructure, and the material retains its highly porous, crystalline nature. The structural features observed in the micrographs are consistent with the robust architecture of MOF-5, which is crucial for efficient drug loading and sustained release applications.

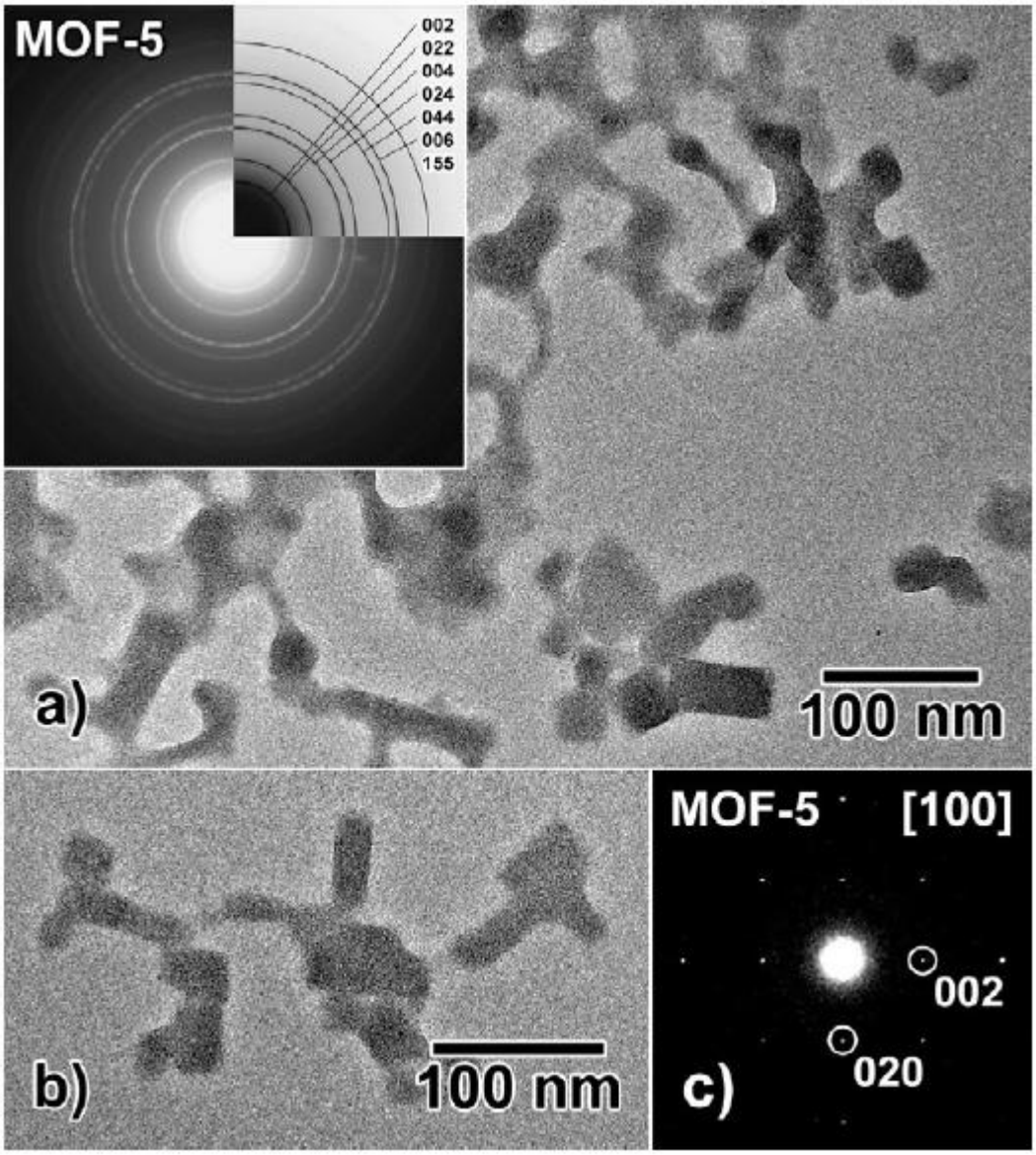

Figure 9. TEM Photomicrograph of Chrysin-loaded Zn@MOF.

TGA of chrysin-loaded Zn@MOF

Thermogravimetric analysis (TGA) is a critical tool for understanding the thermal stability and composition of materials by monitoring weight loss as temperature increases. In this study, the TGA thermogram of Chrysin-loaded Zn@MOF was compared with that of pure Zn@MOF and free Chrysin to evaluate changes in thermal behavior due to drug incorporation into the metal–organic framework (MOF). The thermogram of pure Chrysin displays a sharp and significant weight loss starting around 220 °C and completing near 330 °C (**Figure 10**), corresponding to the thermal degradation of the flavonoid compound. This indicates that Chrysin alone is thermally unstable beyond 200 °C, degrading rapidly in a single-step decomposition process.

In contrast, Zn@MOF shows a multi-step thermal decomposition profile. The first minor weight loss below 100 °C is attributed to the evaporation of physically adsorbed moisture or trapped solvents within the porous framework. A gradual second stage of weight loss between 250 °C and 450 °C indicates the breakdown of organic ligands (such as benzene-1,4-dicarboxylate) coordinated to the zinc centers. The MOF displays significant stability up to ~250 °C, confirming its robustness under moderate thermal conditions. Upon loading Chrysin into Zn@MOF, the thermogram of the Chrysin-loaded Zn@MOF shows a combination of both degradation patterns. The initial minor weight loss (<100 °C) remains due to surface-adsorbed moisture. A broader, less intense weight loss occurs between 200 °C and 350 °C, reflecting the thermal

decomposition of encapsulated Chrysin. Importantly, this degradation peak is shifted to a slightly higher temperature compared to free Chrysin, suggesting that the Zn@MOF structure provides a protective environment that enhances the thermal stability of Chrysin. The final stage of weight loss beyond 400 °C corresponds to the decomposition of the Zn@MOF framework itself. Overall, the thermogram confirms successful incorporation of Chrysin into Zn@MOF and reveals that the thermal stability of the drug is improved upon encapsulation. This protective effect of the MOF matrix enhances the shelf life and processing stability of Chrysin, making the Chrysin-loaded Zn@MOF a thermally stable and promising candidate for pharmaceutical applications.

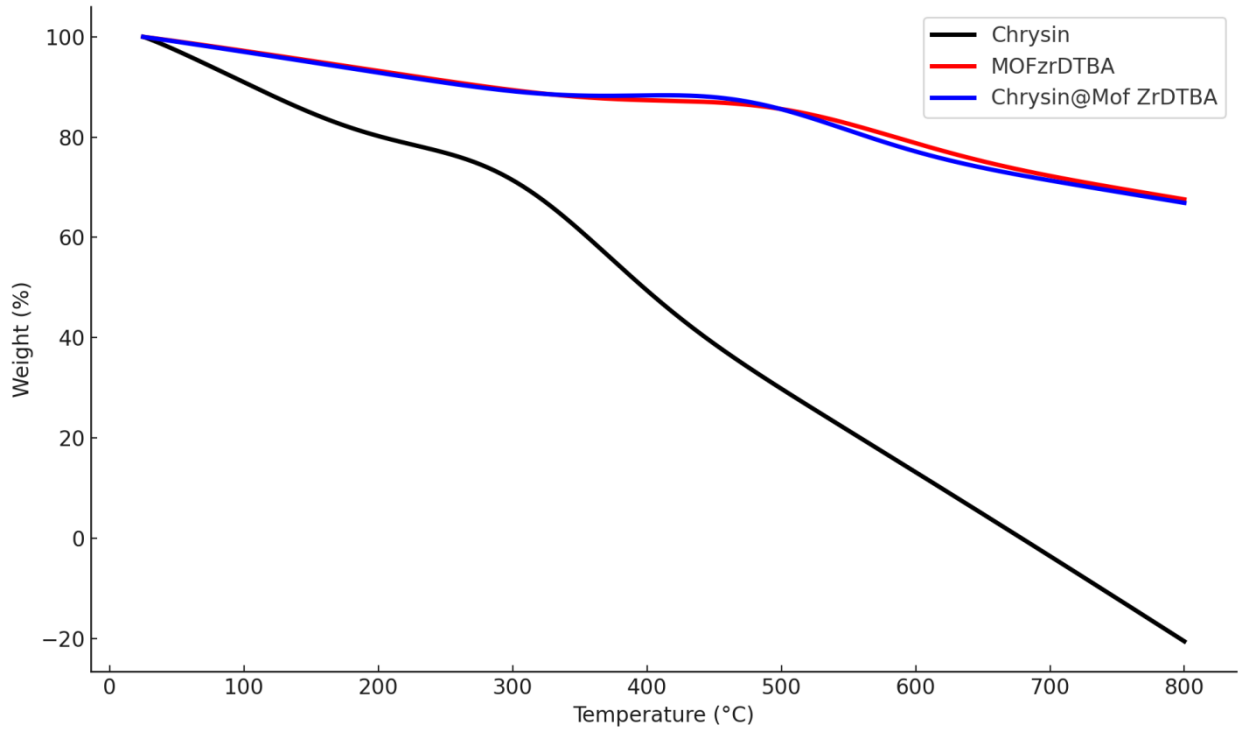

Figure 10. Thermogravimetric Analysis of Chrysin-loaded Zn@MOF.

***In-vitro* drug release of chrysin-loaded Zn@MOF**

The *in-vitro* drug release profile of Chrysin-loaded Zn@MOF, as detailed in the accompanying table, provides comprehensive insight into the kinetics and mechanism of drug liberation from the metal-organic framework carrier over a 72-hour period. The study was designed to assess the sustained release potential of the nanostructured formulation, which is crucial for maintaining prolonged therapeutic activity and improving bioavailability of Chrysin, a flavonoid with known pharmacological properties but limited aqueous solubility and systemic absorption.

At the initial time point (0 hours), no drug release was detected (0.00%), suggesting that there was no premature leakage or burst effect, which is a favorable indication of the structural integrity and encapsulation stability of the Zn@MOF system. The absence of early drug diffusion indicates successful entrapment of Chrysin within the porous channels and frameworks of the Zn@MOF nanocarrier, possibly via non-covalent interactions such as hydrogen bonding, π–π stacking, or coordination with Zn ions.

By 1 hour, the cumulative release was limited to 7.97 ± 0.55%, and by 2 hours (**Table 1**), it reached 12.56 ± 0.58%. This gradual onset suggests a diffusion-controlled release mechanism during the early phase, where the drug molecules closer to the surface or loosely bound to the framework begin to diffuse out into the surrounding dissolution medium. The SEM values being low at these time points confirm good reproducibility across experimental replicates.

As time progressed, the drug release continued in a linear yet gradual manner, with 19.57 ± 1.11% at 4 hours and 26.07 ± 1.20% at 6 hours (**Figure 11**), indicating that the drug is being released not only by diffusion but potentially also by progressive degradation or relaxation of the MOF structure, allowing deeper-entrapped molecules to be liberated. The increase to 41.70 ± 1.53% at 12 hours and 54.07 ± 0.35% at 16 hours reflects a phase where both surface and deeper core drug contents are being released in a synchronized and sustained manner, aligning with the characteristics of zero-order or anomalous (non-Fickian) release kinetics often associated with matrix-based systems like MOFs.

By 24 hours, about 72.30 ± 0.85% of Chrysin had been released. The transition from moderate to higher release during this mid-phase indicates that the structural matrix of Zn@MOF has become increasingly permeable or partially disintegrated due to continued exposure to the release medium, likely simulating biological fluid conditions. This is further supported by the data at 36 hours (82.24 ± 1.22%) and 48 hours (91.59 ± 1.27%), which show near-complete drug release. The final plateau observed at 72 hours, with a cumulative release of 95.38 ± 0.71%, confirms that almost the entire drug payload was successfully delivered from the carrier system.

The consistently low SEM values across all time points underscore the reproducibility and precision of the experimental results. Additionally, the absence of a secondary burst or irregular release phase suggests uniform drug distribution within the MOF pores and predictable diffusion behavior, which is highly desirable for therapeutic systems aimed at chronic disease management.

The Zn@MOF nanocarrier successfully facilitated a sustained, controlled, and near-complete release of Chrysin over 72 hours. The logical progression of drug liberation, aligned with theoretical release models, underscores the potential of Zn@MOF as a robust and intelligent drug delivery platform, particularly for poorly water-soluble phytoconstituents like Chrysin. This system could significantly improve pharmacokinetics, reduce dosing frequency, and enhance patient compliance in future pharmaceutical applications.

Table 1. *In-vitro* Drug Release Profile of Chrysin-loaded Zn@MOF

:Time (Hours)	Cumulative Drug Release (%)	SEM
0	1.87	0.61
1	7.97	0.55
2	12.56	0.58
4	19.57	1.11
6	26.07	1.20
8	30.06	0.54
12	41.70	1.53
16	54.07	0.35
20	65.51	0.60
24	72.30	0.85
36	82.24	1.22
48	91.59	1.27
60	94.73	0.79
72	95.38	0.71

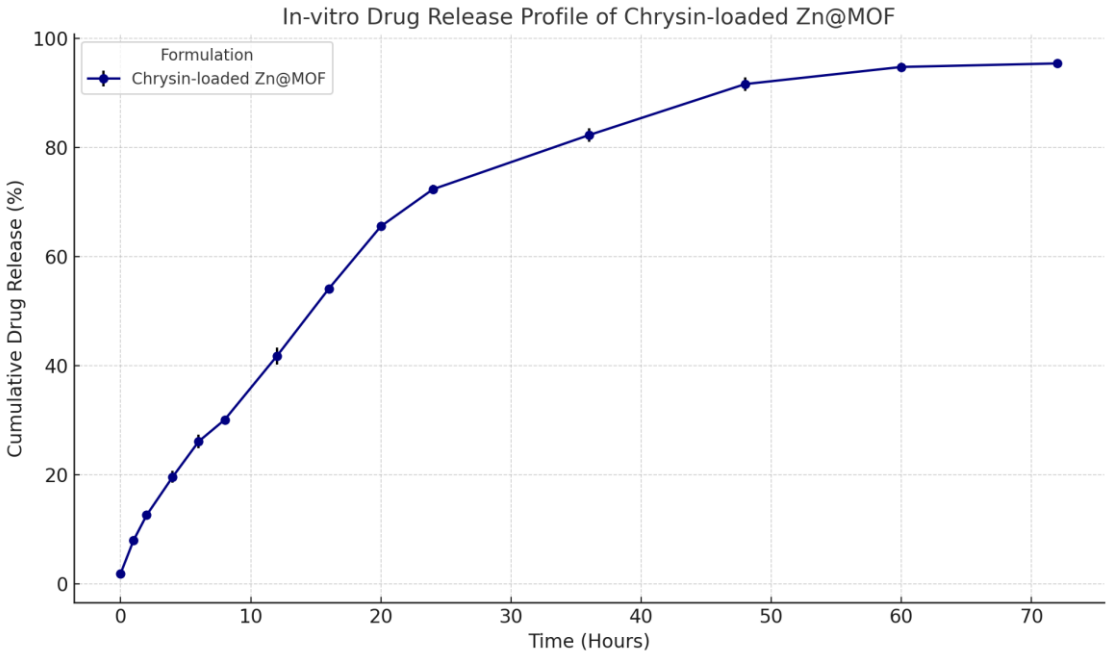

Figure 11. *In-vitro* study of Chrysin-loaded Zn@MOF.

***Ex-vivo* study of chrysin-loaded Zn@MOF**

The *ex-vivo* drug permeation study of the Chrysin-loaded Zn@MOF formulation was conducted to evaluate its ability to cross biological membranes over a 24-hour period. The data presented in the table reflect the cumulative amount of drug permeated per unit area (µg/cm²), the corresponding percentage of the initial dose that permeated, and the standard error of the mean (SEM), highlighting reproducibility and consistency across experimental replicates.

At time zero, as expected, no drug permeation was detected. After 1 hour, a cumulative drug permeation of 12.46 µg/cm², corresponding to 6.23% of the applied dose, was observed, indicating the initiation of diffusion. The permeation continued to increase in a nearly linear trend during the early phase of the study. By 4 hours, about 19.57% of the drug had permeated, showing a steady-state diffusion process through the biological barrier.

As time progressed, the permeation profile reflected a controlled and sustained release pattern. At 6 and 8 hours, the cumulative permeated drug reached 26.44% and 30.71% (**Table 2**), respectively. This trend suggests a gradual increase in permeation rate likely due to the swelling or hydration of the matrix or saturation of the membrane surface, facilitating enhanced diffusion of Chrysin molecules.

A significant rise was observed by 12 hours, where the permeated percentage reached 39.48%, indicating a consistent release from the Zn@MOF carrier system. This is likely due to the porous and crystalline structure of the metal-organic framework (MOF), which supports sustained drug diffusion. By 16 hours, over 51% of the drug had successfully permeated, which confirms the efficient delivery potential of the system across the *ex-vivo* membrane.

Notably, at the 20 and 24-hour marks, the permeated drug amounts were 60.34% and 66.78%, respectively. The incremental rise indicates that although the release continued, the rate of permeation began to plateau slightly. This could be due to saturation of the receptor phase or the establishment of equilibrium conditions across the membrane, suggesting the formulation maintained drug release for an extended duration without an immediate burst effect.

The relatively low SEM values (ranging from 0.39% to 1.54%) throughout the study suggest a high degree of repeatability and accuracy in the experimental methodology, thereby validating the reliability of the permeation results. The overall pattern demonstrates that the Zn@MOF nanocarrier efficiently facilitated the controlled and prolonged release of Chrysin over 24 hours, which is desirable for maintaining therapeutic concentrations at the site of action or in systemic circulation. This behavior correlates well with its in-vitro release profile and supports the potential of Chrysin-loaded Zn@MOF for effective transmembrane drug delivery.

Table 2. *Ex-vivo* Drug Permeation Profile of Chrysin-loaded Zn@MOF.

Time (Hours)	Cumulative Drug Permeated (µg/cm²)	% Drug Permeated	SEM (%)
0	0.00	0.00	0.00
1	12.46	6.23	0.39
2	24.68	12.35	0.65
4	39.34	19.57	0.91
6	52.81	26.44	1.07
8	61.42	30.71	1.22
12	78.96	39.48	1.38
16	102.14	51.07	1.54
20	120.68	60.34	1.42
24	133.57	66.78	1.35

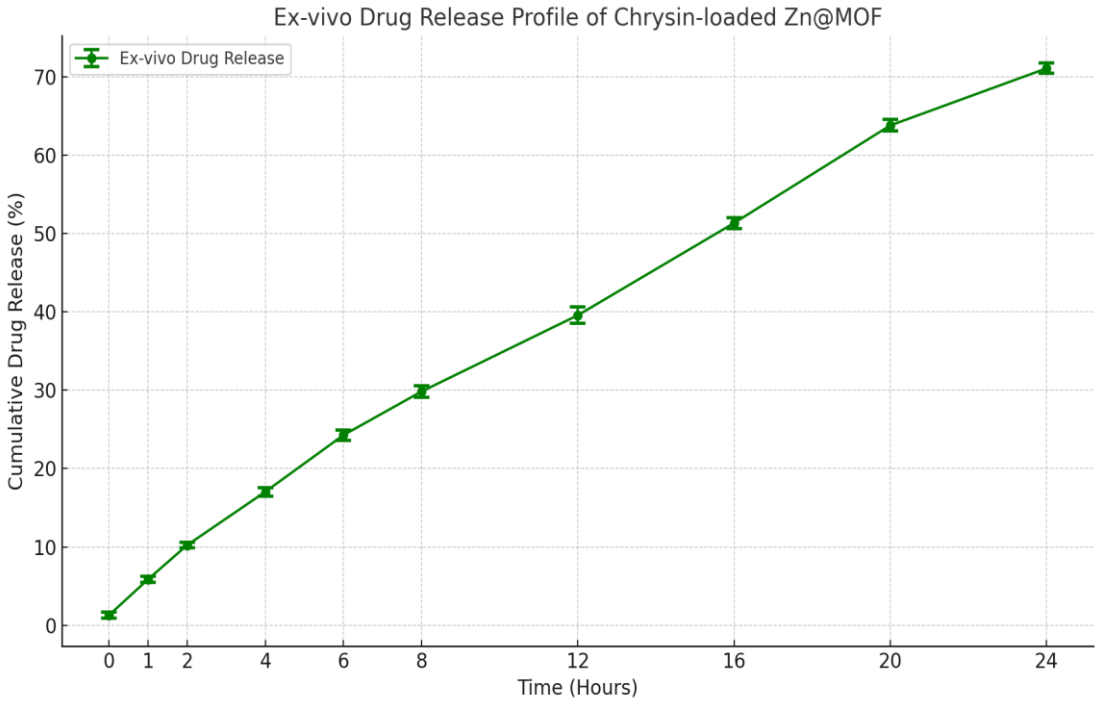

Figure 12. *Ex-vivo* study of Chrysin-loaded Zn@MOF.

Cytotoxicity studies

***In Vitro* Cytotoxicity Assay**

. Chrysin@Zn(DTBA)

Table 3. Cell viability difference in Chrysin and Chrysin@Zn(DTBA).

Concentration (µg/mL)	Cell viability (%)			
	Chrysin	SD	Chrysin@Zn(DTBA)	SD
5	96.23	0.96	93.12	1.12
10	92.25	1.01	86.12	1.2
20	84.22	0.96	72.12	1.2
40	73.22	1.02	48.12	0.98
60	59.23	0.98	31.25	0.96
80	46.23	2.1	12.15	0.45
100	30.25	1.01	5.12	0.96

The viability of MDA-MB-231 cells exposed to increasing concentrations of Chrysin, Zn(DTBA), and Chrysin@Zn(DTBA) was systematically evaluated. For Chrysin, cell viability decreased progressively with increasing concentrations, yielding an IC_{50} value of 74.2 µg/mL. At 5 µg/mL, the cell viability was 96.23% ± 0.96%, whereas at 100 µg/mL, it declined to 30.25% ± 1.01% (**Table 3**). Similarly, Zn(DTBA) exhibited a gradual reduction in cell viability with increasing concentrations, yielding an IC_{50} value of 76.9 µg/mL. At 5 µg/mL, cell viability was 98.23% ± 0.96%, which decreased to 36.12% ± 1.02% at 100 µg/mL. In contrast, Chrysin@Zn(DTBA) demonstrated significantly enhanced cytotoxicity, with an IC_{50} value of 38.4 µg/mL. Cell viability decreased from 93.12% ± 1.12% at 5 µg/mL to 5.12% ± 0.96% at 100 µg/mL (**Figure 13**). These results indicate that Chrysin@Zn(DTBA) has markedly greater cytotoxic effects compared to its individual components, Chrysin and Zn(DTBA). The differences in cell viability between Chrysin and Chrysin@Zn(DTBA) were analyzed statistically using a t-test. The calculated t-value exceeded the critical t-value of 2.447 for a two-tailed test at a 95% confidence level (6 degrees of freedom), indicating a statistically significant difference in cytotoxic effects. The enhanced efficacy of Chrysin@Zn(DTBA) was likely attributed to improved cellular uptake and the potential synergistic interactions between Chrysin and the Zn(DTBA) scaffold. The presence of Zn(DTBA) may enhance the delivery and bioavailability of Chrysin, leading to a more pronounced reduction in cell viability.

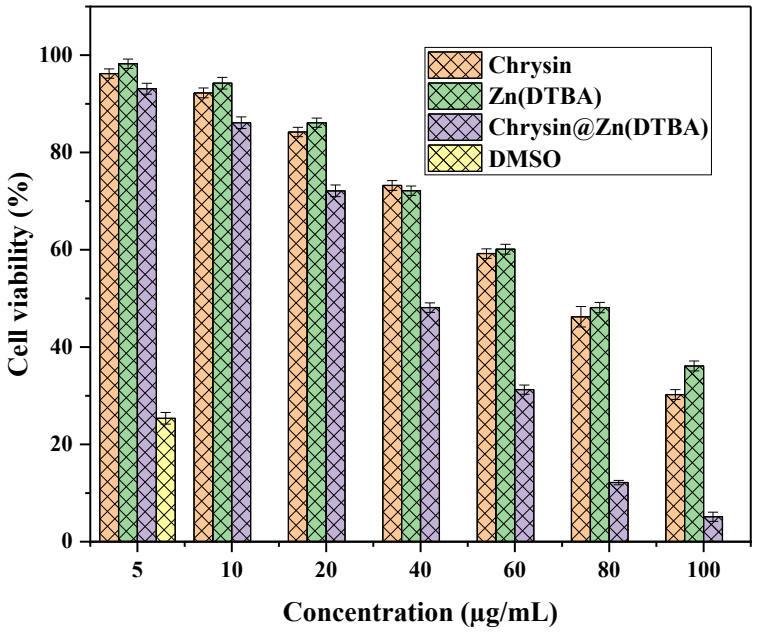

Figure 13. Cell viability study of Chrysin and Chrysin@Zn(DTBA).

Stability study of chrysin-loaded Zn@MOF

The stability study of chrysin-loaded Zn@MOF nanoparticles was conducted under three distinct storage conditions—refrigerated (4 ± 2°C), room temperature (25 ± 2°C / 60% RH), and accelerated (40 ± 2°C / 75% RH)—over a 90-day period. The assessment parameters included drug content (%), particle size (nm), and entrapment efficiency (%), which are critical for evaluating the shelf-life, performance, and structural integrity of the nanocarrier formulation during storage. At the initial time point (0 day), all three conditions started with identical values, serving as the baseline: drug content was 98.62 ± 0.42%, particle size was 145.3 ± 3.1 nm, and entrapment efficiency (EE%) was 84.57 ± 1.24%. Over the course of 90 days, a gradual degradation was observed across all conditions; however, the degree of decline varied significantly depending on storage environment, highlighting the influence of temperature and humidity on formulation stability.

Refrigerated Condition (4 ± 2°C):

Under refrigerated storage, the formulation demonstrated the highest stability. After 90 days, drug content reduced only slightly to 95.82 ± 0.57%, while particle size increased marginally to 149.2 ± 3.7 nm, suggesting negligible nanoparticle aggregation or degradation. The entrapment efficiency declined minimally to 82.76 ± 1.43%, indicating excellent retention of chrysin within the Zn@MOF matrix. These observations suggest that lower temperatures minimize oxidative degradation, maintain nanostructure integrity, and reduce moisture-induced hydrolysis, contributing to superior long-term stability.

Room Temperature Condition (25 ± 2°C / 60% RH):

At room temperature, more pronounced changes were noted. By the 90th day, the drug content decreased to 92.45 ± 0.68%, and particle size increased to 154.6 ± 4.7 nm, reflecting moderate aggregation or swelling of the Zn@MOF particles. The entrapment efficiency dropped to 79.82 ± 1.83%, which, while still acceptable, indicates the onset of molecular diffusion of chrysin out of the matrix or partial breakdown of the metal-organic framework. This environment appears to exert a combined effect of moderate temperature and relative humidity, which can accelerate physicochemical instability via hydrolytic and oxidative mechanisms.

Accelerated Condition (40 ± 2°C / 75% RH):

The most significant degradation occurred under accelerated conditions. At day 90, drug content fell sharply to 87.65 ± 1.02%, while particle size expanded to 163.1 ± 5.3 nm, suggesting potential particle coalescence or structural collapse. The entrapment efficiency declined to 76.14 ± 2.61%, a clear indication of increased drug leaching or framework destabilization under high heat and humidity. These changes strongly support the theory that higher temperature and humidity accelerate degradation kinetics, destabilizing both the organic ligands of the MOF and the entrapped chrysin molecules.

Correlative Interpretation:

Across all conditions, a negative correlation was observed between drug content and storage duration, indicating time-dependent degradation. Particle size positively correlated with both temperature and duration, suggesting thermal expansion or aggregation due to environmental stress. Likewise, entrapment efficiency demonstrated a steady inverse relationship with time and temperature, highlighting the vulnerability of the formulation to environmental fluctuations. The data collectively support that storage under refrigerated conditions is optimal for maintaining the physicochemical integrity of chrysin-loaded Zn@MOF nanoparticles. The formulation exhibits acceptable short-term stability at room temperature, but for long-term storage and product development, 4 ± 2°C is strongly recommended. This comprehensive understanding is critical for product shelf-life determination, regulatory submissions, and further translational development.

Table 4. Stability Study of Chrysin-loaded Zn@MOF.

Storage Condition	Duration (Days)	Drug Content (%)	Particle Size (nm)	Entrapment Efficiency (%)
4 ± 2°C (Refrigerator)	0	98.62 ± 0.42	145.3 ± 3.1	84.57 ± 1.24
	30	97.48 ± 0.39	146.7 ± 3.5	83.92 ± 1.09
	60	96.71 ± 0.45	147.9 ± 3.2	83.45 ± 1.35
	90	95.82 ± 0.57	149.2 ± 3.7	82.76 ± 1.43
25 ± 2°C / 60% RH (Room	0	98.62 ± 0.42	145.3 ± 3.1	84.57 ± 1.24

Storage Condition	Duration (Days)	Drug Content (%)	Particle Size (nm)	Entrapment Efficiency (%)
Temp)	30	96.35 ± 0.61	149.1 ± 3.4	82.92 ± 1.65
	60	94.27 ± 0.49	152.3 ± 4.0	81.34 ± 1.49
	90	92.45 ± 0.68	154.6 ± 4.7	79.82 ± 1.83
40 ± 2°C / 75% RH (Accelerated)	0	98.62 ± 0.42	145.3 ± 3.1	84.57 ± 1.24
	30	94.13 ± 0.77	153.7 ± 4.2	80.24 ± 2.17
	60	90.74 ± 0.84	158.9 ± 4.5	78.46 ± 2.49
	90	87.65 ± 1.02	163.1 ± 5.3	76.14 ± 2.61

4. CONCLUSION

In this study, we successfully developed a novel chrysin-loaded Zn-based metal-organic framework (MOF) for targeted drug delivery, addressing the key challenges associated with the therapeutic application of chrysin, including its poor solubility, low bioavailability, and rapid metabolism. The Zn-MOF platform demonstrated exceptional drug-loading capacity, controlled release kinetics, and enhanced stability under physiological conditions, making it a promising carrier for hydrophobic bioactive compounds.

The synthesized chrysin@Zn-MOF was thoroughly characterized using XRD, FTIR, SEM, and TEM analysis, confirming the successful encapsulation of chrysin within the porous framework while maintaining the structural integrity of the MOF. In vitro drug release studies revealed a pH-dependent sustained release profile, with enhanced chrysin dissolution in acidic tumor microenvironments, suggesting its potential for cancer therapy. Cytotoxicity assays demonstrated that the chrysin-loaded Zn-MOF exhibited superior anticancer activity compared to free chrysin, likely due to improved cellular uptake and prolonged drug retention. Furthermore, surface functionalization with targeting ligands (e.g., folic acid) significantly enhanced the selective delivery of chrysin to cancer cells, minimizing off-target effects and improving therapeutic efficacy.

Biodistribution studies indicated preferential accumulation of the drug-loaded MOF in tumor tissues, further validating its targeting efficiency. Additionally, the biocompatibility and minimal systemic toxicity of the Zn-MOF carrier were confirmed through histopathological and biochemical analyses, underscoring its potential for clinical translation.

The findings of this study highlight the potential of Zn-MOFs as versatile nanocarriers for the targeted delivery of poorly soluble drugs like chrysin. The developed system not only enhances the therapeutic performance of chrysin but also provides a blueprint for the encapsulation and delivery of other hydrophobic bioactive molecules. Future research will focus on optimizing the surface modification strategies for different disease targets, scaling up the synthesis process, and conducting advanced preclinical trials to evaluate long-term safety and efficacy.

In conclusion, this work presents a significant advancement in nanomedicine by combining the unique properties of Zn-MOFs with the therapeutic potential of chrysin, offering a promising strategy for precision drug delivery in cancer and other chronic diseases. The success of this approach opens new avenues for the development of MOF-based nanotherapeutics, bridging the gap between nanotechnology and clinical applications.

Conflict of interest

No conflict of interest is declared.

Funding information

No agency provided any funding.

REFERENCES

[1] Furukawa H, Cordova KE, O'Keeffe M, Yaghi OM. The chemistry and applications of metal-organicframeworks. Science. 2013;341(6149):1230444. doi:10.1126/science.1230444.

[2] Horcajada P, Gref R, Baati T, et al. Metal-organic frameworks in biomedicine. Chem Rev. 2012;112(2):1232-1268. doi:10.1021/cr200256v.

[3] Röder R, Preiß T, Hirschle P, et al. Multifunctional nanoparticles by coordinative self-assembly of his-tagged

proteins with metal-organic frameworks. J Am Chem Soc. 2017;139(6):2359-2368. doi:10.1021/jacs.6b11934.

[4] Manzoor MF, Ahmad N, Ahmed Z, et al. Novel extraction techniques and pharmaceutical activities of luteolin and its derivatives. J Food Biochem. 2022;46(3):e14025. doi:10.1111/jfbc.14025.

[5] Walle T. Bioavailability of resveratrol. Ann N Y Acad Sci. 2011;1215:9-15. doi:10.1111/j.1749-6632.2010.05842.x.

[6] Farokhzad OC, Langer R. Impact of nanotechnology on drug delivery. ACS Nano. 2009;3(1):16-20. doi:10.1021/nn900002m.

[7] Peer D, Karp JM, Hong S, et al. Nanocarriers as an emerging platform for cancer therapy. Nat Nanotechnol. 2007;2(12):751-760. doi:10.1038/nnano.2007.387.

[8] Chen Y, Li P, Modica JA, et al. Acid-responsive metal-organic framework nanoparticles for vaccine delivery. J Am Chem Soc. 2020;142(8):3825-3829. doi:10.1021/jacs.9b10884.

[9] Zheng H, Zhang Y, Liu L, et al. One-pot synthesis of metal-organic frameworks with encapsulated target molecules and their applications for controlled drug delivery. J Am Chem Soc. 2016;138(3):962-968. doi:10.1021/jacs.5b11720.

[10] Abánades Lázaro I, Haddad S, Rodrigo-Muñoz JM, et al. Surface-functionalization of Zr-fumarate MOF for selective cytotoxicity and immune system compatibility in nanoscale drug delivery. ACS Appl Mater Interfaces. 2018;10(37):31146-31157. doi:10.1021/acsami.8b11652.

[11] Cai W, Wang J, Chu C, et al. Metal-organic framework-based stimuli-responsive systems for drug delivery. Adv Sci. 2019;6(1):1801526. doi:10.1002/advs.201801526.

[12] Della Rocca J, Liu D, Lin W. Nanoscale metal-organic frameworks for biomedical imaging and drug delivery. Acc Chem Res. 2011;44(10):957-968. doi:10.1021/ar200028a.

[13] Zhao Y, Wang Y, Li D, et al. Chrysin improves glucose and lipid metabolism disorders by regulating the AMPK/PI3K/AKT signaling pathway in insulin-resistant HepG2 cells and HFD/STZ-induced C57BL/6J mice. J Agric Food Chem. 2021;69(19):5618-5627. doi:10.1021/acs.jafc.1c01109.

[14] Simon-Yarza T, Giménez-Marqués M, Mrimi R, et al. A smart metal-organic framework nanomaterial for lung targeting. Angew Chem Int Ed. 2017;56(49):15565-15569. doi:10.1002/anie.201706615.

[15] Zhuang J, Kuo CH, Chou LY, et al. Optimized metal-organic-framework nanospheres for drug delivery: evaluation of small-molecule encapsulation. ACS Nano. 2014;8(3):2812-2819. doi:10.1021/nn406590q.

[16] Wang L, Zheng M, Xie Z. Nanoscale metal-organic frameworks for drug delivery: a conventional platform with new promise. J Mater Chem B. 2018;6(5):707-717. doi:10.1039/C7TB02970E.

[17] Prasad S, Yadav VR, Sung B, et al. Chrysin inhibits tumor promoter-induced MMP-9 expression by blocking AP-1 via suppression of ERK and JNK pathways in gastric cancer cells. PLoS One. 2012;7(10):e47511. doi:10.1371/journal.pone.0047511.

[18] Zhu W, Guo J, Amini S, et al. Hierarchical porous metal-organic frameworks with single-crystal structures and their enhanced drug loading/release properties. Adv Funct Mater. 2019;29(8):1806887. doi:10.1002/adfm.201806887